Seasonal dependence of localized, high-latitude dayside aurora (HiLDA)

H. U. Frey, N. Østgaard, and T. J. Immel
Space Sciences Laboratory, University of California, Berkeley, California, USA

H. Korth
Applied Physics Laboratory, Johns Hopkins University, Laurel, Maryland, USA

S. B. Mende
Space Sciences Laboratory, University of California, Berkeley, California, USA

Received 15 October 2003; revised 29 December 2003; accepted 23 February 2004; published 7 April 2004.

[1] The FUV instrument on the IMAGE spacecraft frequently observes intense ultraviolet (UV) emissions from a localized High Latitude Dayside Aurora (HiLDA) poleward of the general auroral oval location [*Frey et al.*, 2003a]. It has been shown that this aurora is entirely created by high-energy precipitating electrons, which have probably been accelerated in a quasi-static field-aligned electric potential. Here we extend the previous case study to an investigation of the HiLDA occurrence in the Northern Hemisphere over more than 2 years and compare it with the averaged solar wind plasma and interplanetary magnetic field (IMF) properties. HiLDA occurrence is strongly biased toward low solar wind density and IMF with positive B_z, strong positive B_y (clock angles around 70°), and negative B_x components. Such IMF conditions are favorable for lobe reconnection in the Northern Hemisphere, and the creation of a dominating dusk convection cell with an upward field-aligned current in its center. Additionally, we investigate the seasonal occurrence of this phenomenon, which shows a maximum in the Northern Hemisphere during sunlit summer months and an almost complete absence in the dark winter. In contrast to the daylight-suppressed aurora in the auroral oval, the HiLDA cannot be the result of ionospheric feedback due to the stronger ionospheric conductance in sunlight. Instead, in agreement with ionospheric convection models, it is caused by the asymmetry of field-aligned currents in different seasons, which result from the different dipole tilt angles in summer and winter. We further discuss two scenarios for how the low solar wind density can enhance the field-aligned parallel potential over the dusk convection cell. *INDEX TERMS:* 2704 Magnetospheric Physics: Auroral phenomena (2407); 2708 Magnetospheric Physics: Current systems (2409); 2716 Magnetospheric Physics: Energetic particles, precipitating; 2776 Magnetospheric Physics: Polar cap phenomena; *KEYWORDS:* cause, high-latitude aurora, seasonal dependence

Citation: Frey, H. U., N. Østgaard, T. J. Immel, H. Korth, and S. B. Mende (2004), Seasonal dependence of localized, high-latitude dayside aurora (HiLDA), *J. Geophys. Res.*, *109*, A04303, doi:10.1029/2003JA010293.

1. Introduction

[2] The aurora generally occurs in an oval between 60°–75° magnetic latitude in both hemispheres. In addition, there are many other types of localized aurora at high latitude separated from the auroral oval. Polar-cap patches drift in the anti-sunward direction [see, e.g., *Walker et al.*, 1999]. Poleward moving auroral forms separate from the dayside auroral oval, move poleward for several minutes, and disappear inside the polar cap [*Sandholt et al.*, 1986]. Many different kinds of arc-like features in the polar cap have been reviewed and summarized [*Zhu et al.*, 1997; *Kullen et al.*, 2002]. These features appear during northward IMF conditions and are described as sun-aligned arcs, transpolar arcs, or theta-aurora. They appear mostly during quiet geomagnetic conditions.

[3] Large-scale dayside auroral features were described by *Murphree et al.* [1990] during periods of northward IMF with IMF $B_x < 0$ and $B_y > 0$. Several of their observations showed that transpolar arcs were connected to localized emission regions, which lead them to conclude that these regions were connected to the high-latitude magnetopause, poleward of the cusp. In a later study, *Elphinstone et al.* [1993] summarized the dayside auroral features recorded by the UV imager on Viking. They demonstrated the relation of westward and anti-sunward motion of high-latitude dayside auroral forms in the northern post-noon region with anti-parallel merging occurring poleward of the cusp on the front surface of the magnetotail.

0148-0227/04/2003JA010293$09.00

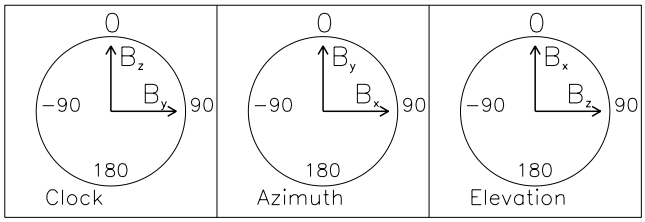

Figure 1. Definitions of solar wind clock angle $\theta = atan(B_y, B_z)$, azimuth angle $\phi = atan(B_x, B_y)$, and elevation angle $\alpha = atan(B_z, B_x)$ in GSM coordinates as they will be used in Figure 5.

[4] *Ohtani et al.* [1997] extended an earlier investigation of dayside aurora by *Murphree and Elphinstone* [1988] with IMF, ground magnetometer, and DMSP satellite particle data and showed the response of a localized aurora spot to changes in the IMF. The solar wind density and velocity corresponding to the observation of the auroral spot were quasi-steady prior to and during its appearance. A sudden increase in the positive IMF B_z was determined as the cause of the spot.

[5] There is also the aurora at the footprint of the cusp that occurs at different magnetic latitudes for northward and southward IMF [*Carbary and Meng*, 1986]. The origin of the cusp aurora from magnetopause reconnection and the different location of the reconnection site for northward (southward) IMF at the high (low) latitude causes different morphology, location, and brightness of the cusp aurora [*Frey et al.*, 2002, 2003c]. During northward IMF the aurora at the cusp footprint occurs in a spot-like area and is sometimes completely separated from the auroral oval.

[6] In a recent study, a localized High-Latitude Dayside Aurora (HiLDA) was described together with an analysis of solar wind properties during 13 events in April–June 2001 [*Frey et al.*, 2003a]. It is created by energetic electrons (several keV) and lacks any signature of simultaneous proton precipitation. It shows brightness changes on timescales between 30 and 70 min and occurs during very low solar wind density/pressure and northward IMF with a positive B_y component. This aurora was explained as a consequence of high-latitude magnetopause reconnection that drives a downward current into the cusp footprint. This current is closed by an upward field-aligned current poleward of the cusp originating from the ionospheric HiLDA location. During low solar wind density, the abundance of current carriers (electrons) is very low and the system sets up an electrostatic potential to drive the few existing current carriers to close the current flow [*Frey et al.*, 2003a; *Korth et al.*, 2004]. The interpretation of the high-latitude reconnection process as the driving mechanism for the HiLDA occurrence was also consistent with observations and modeling of the high-latitude convection during northward IMF with strong B_y component [*Le et al.*, 2002].

[7] Here we are going to extend the previous case studies to a more general relationship of HiLDA with solar wind conditions and investigate the seasonal occurrence of this phenomenon in the Northern Hemisphere. After a brief summary of instrumentation and IMAGE FUV observations we extend the previous case studies to a full 2-year period and discuss seasonal differences of the occurrence frequency of HiLDA.

2. Instrumentation and Data Analysis

[8] The IMAGE satellite is in a highly elliptical polar orbit of 1000 × 45,600 km altitude. The Far Ultra-Violet imager (FUV) consists of three imaging sub-instruments and observes the aurora for 5–10 s during every 2-min spin period [*Mende et al.*, 2000]. Major properties such as fields of view, spatial resolution, and spectral sensitivity were validated by in-flight calibrations with stars [*Frey et al.*, 2003b]. The Wideband Imaging Camera (WIC) has a passband of 140–180 nm covering emissions from the N_2 LBH-band and atomic NI lines. The proton aurora imaging spectrographic imager channel (SI-12) is sensitive to the Doppler-shifted Lyman-α emission around 121.8 nm from charge exchanging precipitating protons [*Frey et al.*, 2001]. The oxygen imaging spectrographic imager channel (SI-13) has a passband of 5 nm around the 135.6-nm doublet of oxygen OI emission.

[9] Solar wind parameters for this study were obtained through CDAWeb from the Wind and ACE spacecraft. All solar wind properties were propagated to their most likely ionospheric impact times using the method described by *Jacobsen et al.* [1995]. In this method the solar wind is propagated to the bow shock with the solar wind speed, the magnetosheath velocity is averaged as 1/8 of the solar wind speed, and a single Alfvén travel time is used along the magnetic field line down to the ionosphere. Uncertainties amount to a few minutes and should not cause large errors in this investigation as the HiLDA spots were observed for long times (20–600 min) during mostly stable solar wind

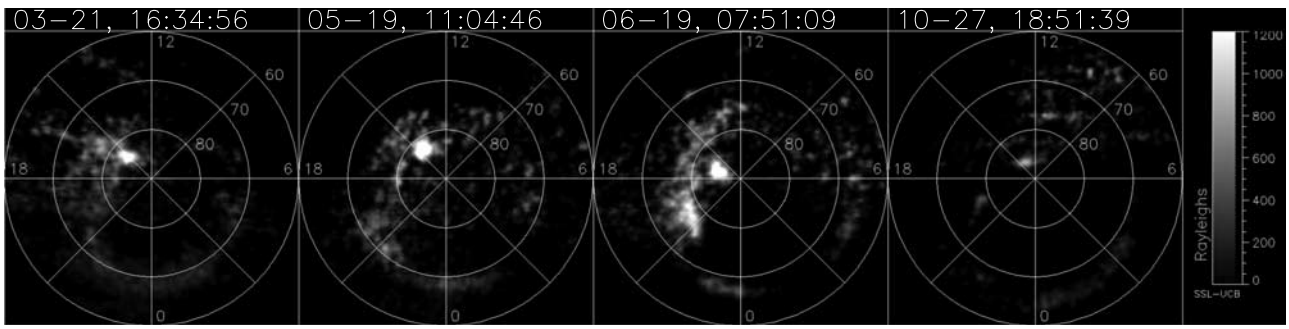

Figure 2. Examples of Northern Hemisphere HiLDA observations by WIC for four different days in 2001. The original images were re-mapped into an MLT-latitude grid with local noon at the top, midnight at the bottom, and dawn to the right of each image.

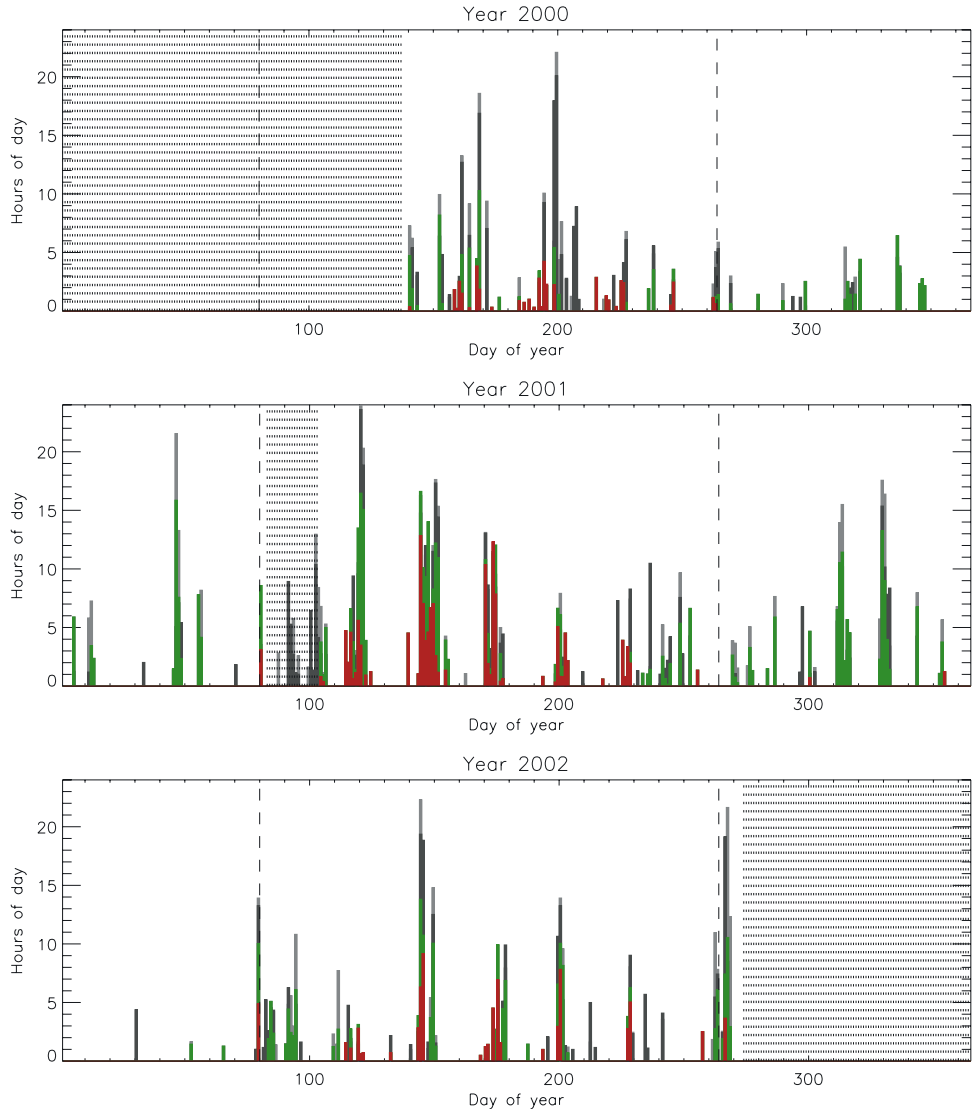

Figure 3. Statistical summary of HiLDA observations and favorable solar wind conditions. For every day in 2000–2002, a gray/black bar indicates favorable solar wind conditions as measured by Wind/ACE. Green bars indicate how long during these times FUV provided auroral images of the northern polar cap. Red bars show how long HiLDA was observed in FUV. Horizontally lined areas exclude the times without FUV observations, and the vertical dashed lines indicate vernal and autumnal equinox.

conditions. All magnetic field data were transformed into the GSM coordinate system. The solar wind clock, azimuth, and elevation angles in GSM-coordinates as they will be used later in this study are schematically given in Figure 1.

3. Solar Wind and FUV Observations

[10] Examples of HiLDA observations from four different days in 2001 are given in Figure 2. The original images were dayglow corrected and then re-mapped into a geomagnetic latitude-MLT coordinate system. Some of the images show small portions of the auroral oval with weak emissions, but in most cases of HiLDA observations, large portions of the auroral oval are very dim and the brightness is below the sensitivity limit of WIC (about 300 R).

[11] During the time period of May 19, 2000 (start of regular IMAGE-FUV operations), to September 30, 2002, we searched for favorable solar wind conditions which, according to the previous study, should be favorable for the occurrence of HiLDA [*Frey et al.*, 2003a]. In solar wind data measured by Wind and ACE time periods were selected which fulfilled the following criteria: (1) The solar wind proton density had to be less than 3 cm^{-3}, (2) the GSM-B_z component had to be greater than -0.5 nT, and (3) these conditions had to be fulfilled for more than 60 min.

[12] We decided to relax the requirement for positive GSM-B_z to values greater than -0.5 nT instead of greater than 0.0 nT to allow for short-duration minimal negative excursions to still be included into the database. We excluded times when Wind was inside the magnetosheath/magnetosphere. A total of 1057 hours were found in Wind data which fulfilled the selection criteria, and a total of 770 hours with appropriate ACE data. The smaller number of hours with ACE data is caused by large data gaps in ACE measured solar wind density and velocity. Figure 3 summarizes these results. For every day the total time is given for

which the selection criteria were fulfilled in Wind (gray bars) and ACE data (black bars). The shaded areas indicate time periods when there were no FUV data available before launch, during a 2-week break in operation, and after the end of the present study period (30 September 2002). For each of these time periods we checked how long FUV did operate and provided images of the Northern Hemisphere polar cap. The result is given as green bars in Figure 3.

[13] Additionally, we visually inspected the full IMAGE-FUV data set for time periods which fulfilled the following criteria: (1) A localized region of bright emission had to be found poleward of the dayside auroral oval (>70° magnetic latitude) in the WIC images, (2) the localized region had to be observable for at least 20 min, and (3) no signature of proton precipitation is allowed in the SI-12 images.

[14] The third criterion eliminated several time periods of proton precipitation into the cusp similar to those previously described by *Frey et al.* [2002]. The total times with HiLDA observations are shown with red bars in Figure 3. The most obvious result is the complete absence of HiLDA in January-mid-March and the rare occasion in October–December with only two brief periods of HiLDA observations during the two northern winter seasons. There is a maximum of HiLDA occurrence in the northern summer months when the phenomenon could be observed for many hours and sometimes repeatedly during the same day. In contrast, there are only two HiLDA observations on October 27 and December 20, 2001, though the general solar wind conditions were favorable for long times on many other days, especially in February and November 2001. A summary of the dates and times which were used to produce Figure 3 is published as an electronic supplement on the AGU web site for the scientific community to further explore this phenomenon and compare it with their own measurements.[1]

4. FUV Observations and Relationship to Solar Wind Properties

[15] Several individual events of HiLDA observations were described by *Frey et al.* [2003a]. Here we want to investigate a few additional statistical properties for the occurrence of HiLDA and especially extend it to over 2 years of observation.

[16] The average geomagnetic locations of the HiLDA spots are summarized in Figure 4. The center locations of the spots were determined once every 15 min, and the result is shown in histogram format in geomagnetic latitude and local time. The maximum probability of HiLDA observations occurs at 84.5° latitude and 1430 hours MLT. The latitude is on average 10° higher than that of the postnoon auroral bright spots that were observed by the Polar UVI instrument [*Liou et al.*, 1999]. Simultaneous particle measurements identified the source region of these 1500 MLT bright spots as the plasma sheet with keV-energy electrons together with energetic, hot, dense plasma sheet ions. In contrast, particle measurements at HiLDA spots showed a complete absence of precipitating ions [*Frey et al.*, 2003a],

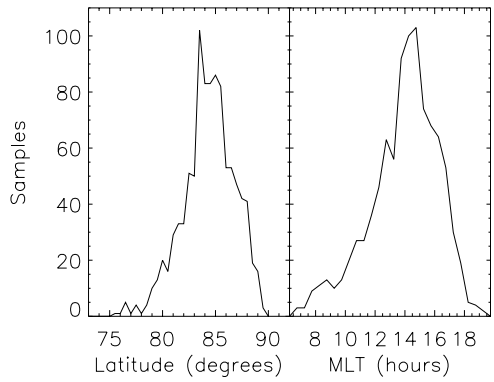

Figure 4. Summary of the geomagnetic locations of the HiLDA spots. The center location of each spot was determined once every 15 min. The observations are shown in histogram format in bins of 0.5° geomagnetic latitude and 0.5 hours local time.

and indicate that the 1500 MLT spot and HiLDA are two different phenomena.

[17] Figure 5 summarizes the statistical solar wind density and magnetic field properties observed in 2000–2002 by the Wind and ACE spacecraft and relates them to the occurrence of HiLDA. We separate the FUV observations related to the Wind or ACE measurements as the solar wind monitors often show different solar wind properties (magnitude and direction of the IMF) and their number of measurements differ due to magnetospheric passages by Wind and large data gaps from ACE. For the comparison of HiLDA observations the solar wind measurements were propagated to their estimated time of ionospheric impact, and those falling into the HiLDA observation intervals are summarized in histogram format as black curves in Figure 5. The corresponding histograms of solar wind measurements were then normalized to the maxima of the HiLDA related measurements, and are shown as shaded curves.

[18] The top two panels of Figure 5 show the histograms for the IMF clock angle $\theta = atan(B_y, B_z)$. The averaged clock angle over 3 years shows two peaks around −90° and +90° due to the general Parker spiral geometry of the solar wind magnetic field with a dominating *y*-component compared to the *z*-component. Out of this symmetric behavior the HiLDA occurrence prefers clock angles around 60°–70°, again confirming the previous result of preferred large positive B_y and small, positive B_z.

[19] The next two panels of Figure 5 show the IMF azimuth angle here defined as $\phi = atan(B_x, B_y)$. The general Parker spiral solar wind magnetic field geometry causes two maxima at −45° and +135° for equal magnitudes and opposite directions of the B_x and B_y components. Out of these values, HiLDA preferably occur at azimuth angles around −30° with larger positive B_y values than the absolute value of the negative B_x.

[20] For completeness we also show the IMF elevation angle defined as $\alpha = atan(B_z, B_x)$. Again, there are two maxima at 0° and 180° caused by the Parker spiral geometry. The HiLDA occur preferably at values around 160° with larger negative B_x and positive B_z values. That again suggests the previous conclusion that HiLDA are driven by the high-latitude anti-parallel reconnection in the Northern

[1] Auxiliary material is available at ftp://ftp.agu.org/apend/ja/2003JA010293.

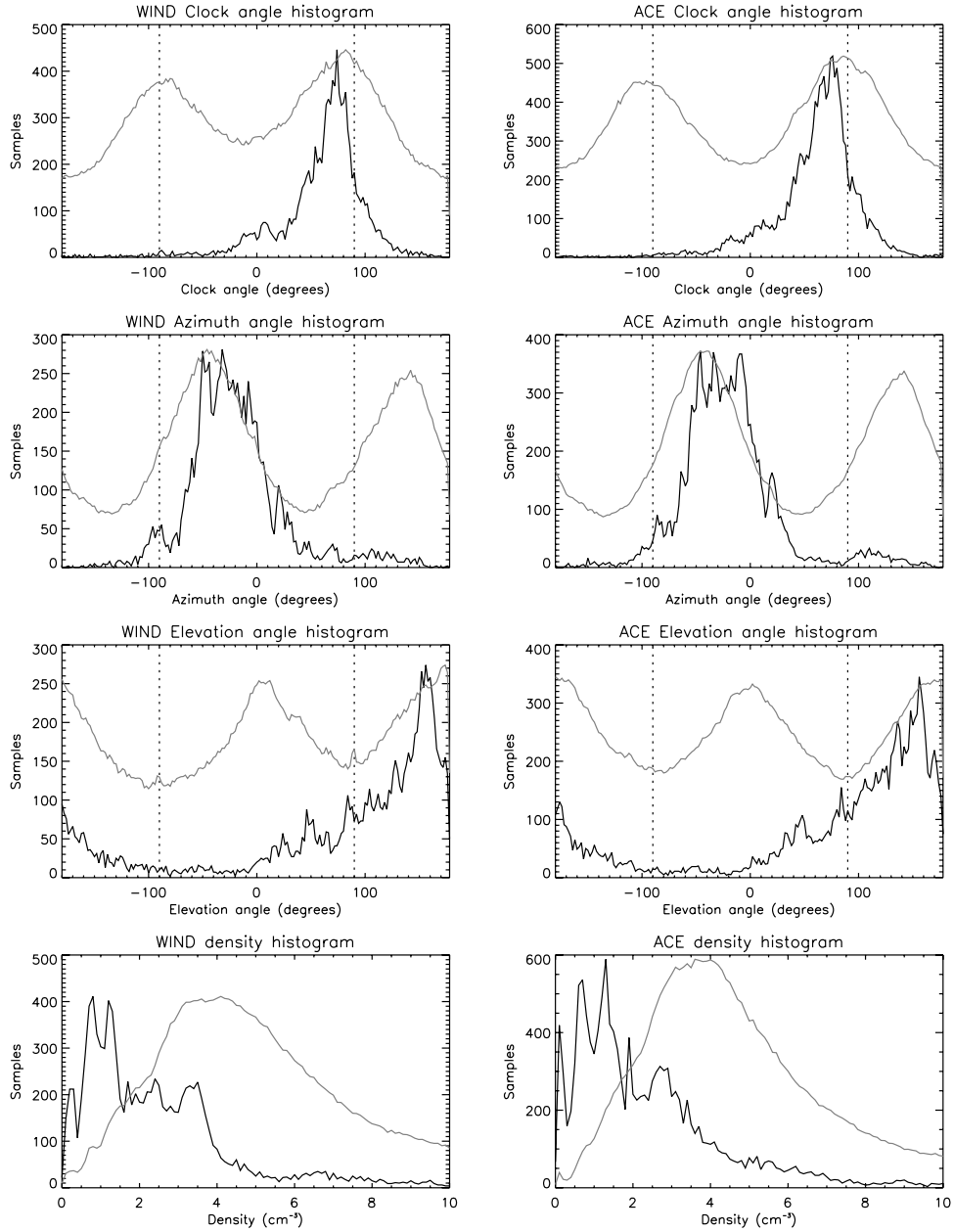

Figure 5. Summary histograms of all solar wind conditions between 2000 and 2002 (shaded lines) and the comparison with solar wind parameters during the observation of HiLDA (black lines). The left and right columns show the solar wind properties as measured by Wind and ACE spacecraft, respectively. There were more than 1 million valid IMF measurements by Wind (92-s resolution) and almost 6 million by ACE (16-s resolution). There were almost 1 million valid solar wind plasma measurements by Wind (97-s resolution) and almost 1.5 million by ACE (64-s resolution). The top three rows summarize the IMF magnetic field clock, azimuth, and elevation angles, respectively. All angles were binned in 2° bins. The bottom row shows the histogram of solar wind density binned into 0.2 cm^{-3} bins. The solar wind histograms were normalized to the maxima of HiLDA observation histograms.

Hemisphere with positive B_z, negative B_x, and an additional strong positive B_y.

[21] The two bottom panels summarize the solar wind density properties. The Wind and ACE data have similar median values of 5.2 and 4.7 cm^{-3}, and mean values of 7.0 and 6.2 cm^{-3}, respectively. HiLDA preferably occurs during low solar wind density, and therefore the density histogram is shifted toward lower values with similar mean and median values of 2.7 cm^{-3} and 2.0 cm^{-3} for both solar wind monitors.

5. Discussion

[22] An interesting observation is the periodicity of roughly 27 days of HiLDA observations, especially in summer 2001 and 2002, that is similar to the solar rotation

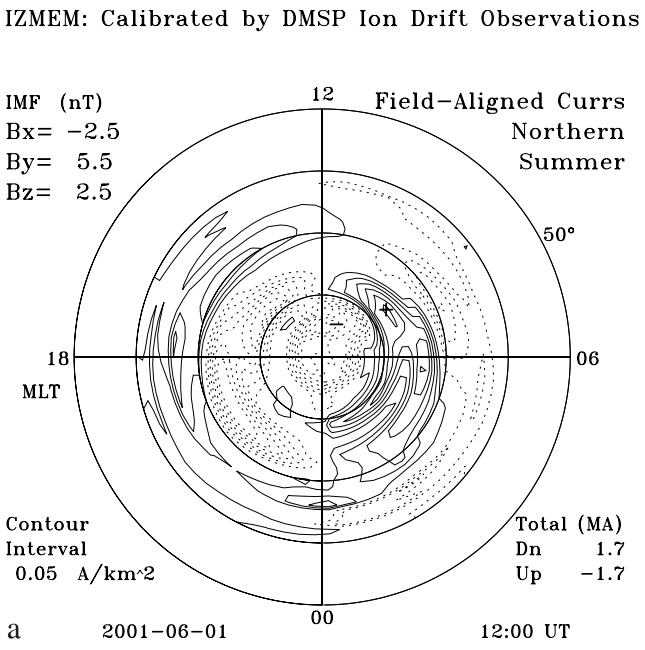

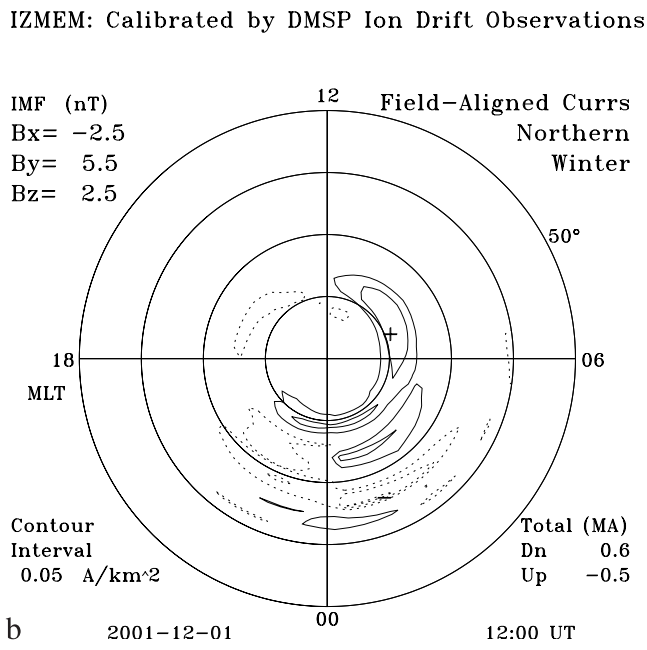

Figure 6. Results of model calculations of the field-aligned current distribution with the IZMEM model calibrated by DMSP ion drift observations [*Papitashvili and Rich*, 2002]. Input parameters were the average solar wind magnetic field values for HiLDA observations, and the calculations were performed for northern summer and winter, respectively.

period. The periods of frequent HiLDA observations coincided with periods of low geomagnetic activity (small Kp 0–2) most likely caused by a region of low solar activity and its sector in the Parker spiral of the solar magnetic field. This observation confirms that HiLDA is not a phenomenon of strong geomagnetic activity but occurs rather during quiet conditions with northward IMF and low solar wind density.

[23] The major open question for this investigation is the reason for the preferred occurrence during the northern summer months. It cannot be attributed to a more frequent occurrence of favorable solar wind conditions during the summer months, as our Figure 3 indicates extended periods with favorable conditions in February and November 2001 without HiLDA observations.

[24] The two most important ionospheric/magnetospheric properties that are different in summer and winter are the ionospheric conductance and the dipole tilt angle. The general location of HiLDA at the dayside and 80°–90° latitude is in full sunlight during summer and in darkness during winter. In a statistical study of electron precipitation in the auroral oval, *Newell et al.* [1996] found that beams of accelerated electrons creating discrete aurora occur primarily in darkness. The winter hemisphere is favored over the summer hemisphere, and night is favored over day. Solar EUV radiation increases the ionospheric conductivity during summer [see, e.g., *Foster et al.*, 1983], allowing field-aligned currents to flow without potential drop and electron acceleration. The authors therefore concluded that the ionospheric feedback mechanism controls the occurrence of discrete aurora with the lowest occurrence probability in the sunlit ionosphere. Numerical MHD model calculations confirmed that conclusion with a larger electron energy flux into the winter hemisphere [*Pokhotelov et al.*, 2002]. A similar anti-correlation between ionospheric conductance and discrete aurora brightness was obtained with Polar UVI images [*Shue et al.*, 2001]. Here we find a completely opposite behavior of HiLDA. The preferred occurrence in the sunlit summer hemisphere must have a different cause than the ionospheric conductance effect on the development of the feedback instability.

[25] The largest positive dipole tilt angles occur in northern summer, and the largest negative tilt angles occur in northern winter. Ionospheric properties that respond to changes in the dipole tilt are the distributions of the ionospheric electric potential and field-aligned currents [*Papitashvili et al.*, 1994; *Weimer*, 2001]. As an example, we present the distribution of field-aligned currents as calculated by the IZMEM model calibrated by DMSP satellite ion drift observations in Figure 6 [*Papitashvili and Rich*, 2002]. We used as input parameters the mean solar wind values during the HiLDA observations (section 4) which were $B_x = -2.5$ nT, $B_y = 5.5$ nT, and $B_z = 2.5$ nT. The IZMEM model is not parameterized for solar wind density or pressure. We then calculated the distribution of field-aligned currents on June 1 and December 1, 2001.

[26] Figure 6a shows the field-aligned current distribution during northern summer. Solid lines indicate contours of downward current, and dashed lines indicate contours of upward current. During these conditions with a strong positive B_y a two cell convection pattern forms with the upward field-aligned current located at high latitude in the center of a clockwise convection dusk cell.

[27] Figure 6b shows the field-aligned current distribution during northern winter. The high-latitude region-1 and dayside upward field-aligned currents are much larger in summer than in winter. The same also applies to the downward field-aligned currents as the pairs are well

balanced [*Christiansen et al.*, 2002]. However, these downward field-aligned currents do not show auroral features that would be visible in our ultraviolet images. This general increase of the field-aligned currents in summer is likely one of the major reasons for an increased occurrence of HiLDA with increased currents in the summer season.

[28] The whole process of HiLDA generations appears to be a combination of several effects. When the IMF has a strong positive B_y component and the dipole has a large positive tilt angle, the dusk cell dominates the dawn cell in the northern summer hemisphere so that it almost disappears [*Crooker and Rich*, 1993]. This also creates an upward current at high latitude in the center of the dusk convection cell [*Eriksson et al.*, 2002]. Additional positive IMF B_z and negative B_x components favor reconnection tailward of the northern cusp [*Luhmann et al.*, 1984], with a possible B_y-related shift toward the dusk flank, and drive a downward current into the dayside cusp. The high ionospheric conductance from solar EUV illumination of the northern polar cap allows the downward current in the cusp to connect with the upward current poleward of it.

[29] The impact of the low solar wind density may be twofold. If the solar wind density is low, or even more if it has been low for some time, the tail region of the magnetosphere does not have enough current carriers to maintain the upward current. In order to keep the current flowing [*Siscoe et al.*, 2001], the system sets up a parallel potential that accelerates the electrons into the ionosphere and subsequently creates the HiLDA at the footprint. The other possible impact of the low solar wind density is the reduction of the Alfvén Mach number and a lower plasma beta in the magnetosheath adjacent to the reconnection site. The reduced Mach number enhances the strength of the dusk convection cell [*Crooker et al.*, 1998] and thus the strength of the upward current at the HiLDA footprint. The lower plasma beta is considered favorable for the onset of reconnection and can create a stronger downward current into the cusp. A lower Mach number would also enhance the probability of sunward convective components in the reconnected open flux tubes due to the $j \times B$ forces overcoming the tailward tugging of the magnetosheath field [e.g., *Gosling et al.*, 1991; *Cooling et al.*, 2001].

[30] The whole process can therefore be explained with two slightly different scenarios. The first possibility is that (1) as a result of the large positive dipole tilt, (2) a strong dusk convection is driven, with (3) the positive IMF B_z creating reconnection, that (4) drives the downward current, which (5) is closed by the high ionospheric conductance to the (6) field-aligned upward current, which (7) requires acceleration of electrons due to the low density of available current carriers. The other possibility is that (1) a large dipole tilt for $B_y > 0$ enhances (2) the probability of reconnection and the offset of the merging site toward the duskside flank, which (3) together with a low solar wind density results in (4) a stronger dusk convection cell with a higher potential drop over it that generates (5) a stronger upward current that (6) closes more easily via Pedersen currents in the summer northern ionosphere. The available data do not allow ruling out one or the other of the two possibilities. However, regardless of which option is true, the HiLDA creation process is different from the creation of discrete aurora by the feedback instability, which occurs during low ionospheric conductance [*Newell et al.*, 1996].

6. Conclusions

[31] We extended a previous event investigation of the properties of localized, bright FUV emission at the dayside high latitudes, which are frequently observed by the FUV instrument on IMAGE [*Frey et al.*, 2003a]. The much higher latitude location, the requirement for low solar wind densities and strong positive IMF B_y, and the complete absence of proton precipitation separate this phenomenon from the previously described proton aurora in the cusp [*Frey et al.*, 2002] and the 1500 MLT bright aurora spot [*Liou et al.*, 1999].

[32] This paper compares the general occurrence of HiLDA over more than 2 years of IMAGE observations with the average solar wind conditions during that time. It is found that the HiLDA occurrence has a very different magnetic field and solar wind density distribution than the averaged solar wind properties. This confirms that there are favorable solar wind conditions that act as a driver for this phenomenon and other conditions, which completely suppress the occurrence. The favorable HiLDA conditions are as follows: (1) The solar wind proton density had to be less than 4 cm^{-3}, preferably even less than 2 cm^{-3}; (2) the IMF clock angle has to be between 50° and 90°; and (3) the IMF azimuth angle has to be between −60° and 0°.

[33] Furthermore, we show here for the first time a very strong seasonal dependence of HiLDA occurrence with a maximum in northern polar summer and a minimum in northern winter. In contrast to the preferred occurrence of aurora in the auroral oval during darkness [*Newell et al.*, 1996], this phenomenon has an opposite behavior and cannot be caused by the ionospheric conductance feedback.

[34] The other major ionospheric properties with a seasonal dependence are the distributions of electric potentials and field-aligned currents with different dipole tilt angles [*Papitashvili et al.*, 1994; *Weimer*, 2001]. In addition to the conclusion in the previous paper that high-latitude reconnection is the driving process of HiLDA creation, we here confirm with semi-empirical model calculations that the seasonal differences in dipole tilt and field-aligned current strength are the driving factors for the seasonal dependence of HiLDA occurrence. During northern winter, when the field-aligned current strength is small, there is no need for the magnetosphere/ionosphere system to set up a strong field-aligned parallel potential to drive the upward current to the HiLDA footprint. In northern summer the field-aligned current strength is high and the high ionospheric conductance allows for an efficient current closure. The system either requires a parallel potential during times of low solar wind density, to compensate for the lack of current carriers and drive the required upward field-aligned current which in turn creates the bright, localized aurora

[*Korth et al.*, 2004]. The other possibility is a stronger potential drop over the dominating dusk convection cell due to the increased reconnection in response to the lower magnetosheath Alfvén Mach number and plasma beta.

[35] Whether the upward currents at HiLDA close with the downward cusp currents or not, however, cannot be fully answered based on the evidence provided in this paper alone. It has been suggested that a dominant IMF B_y rotates the magnetotail and may push the boundary plasma sheet poleward on the northern duskside for positive IMF B_y [e.g., *Meng*, 1981; *Siscoe and Sanchez*, 1987; *Cowley et al.*, 1991; *Jankowska et al.*, 1990]. That suggests the possibility of a connection of HiLDA with the postnoon lower latitude boundary plasma sheet. The role of the enhanced summertime ionospheric conductivity would thus be to close the imposed upward current via Pedersen currents to the region 2 downward current equatorward of the boundary plasma sheet. It may therefore be that the upward current closes with both systems of downward currents.

[36] A file summarizing all time periods used for this study is available as an electronic supplement.[1] Other researchers are invited to look at those time periods with their data and different instrumentation.

[37] **Acknowledgments.** We thank V. Papitashvili for developing a web-based interactive interface to the Linear Models of Ionospheric Electrodynamics and making it available at http://maggy.engin.umich.edu/mist/. The IMAGE FUV investigation was supported by NASA through SwRI subcontract 83820 at the University of California at Berkeley under contract NAS5-96020. The solar wind measurements were obtained from CDAWeb. We acknowledge the following PIs: Wind Magnetic Fields Investigation: R. Lepping; Wind Solar Wind Experiment: K. Ogilvie; ACE Magnetic Field Instrument: N. Ness; and ACE Solar wind experiment Instrument: D. J. McComas. We are indebted to K. Trattner and S. Claflin for providing the files with solar wind data.

[38] Arthur Richmond thanks F. Christiansen and Stefan Eriksson for their assistance in evaluating this paper.

References

Carbary, J. F., and C. I. Meng (1986), Correlation of cusp latitude with B_z and AE(12) using nearly 1 year's data, *J. Geophys. Res.*, *91*, 10,047.

Christiansen, F., V. O. Papitashvili, and T. Neubert (2002), Seasonal variations of high-latitude field-aligned currents inferred from Ørsted and Magsat observations, *J. Geophys. Res.*, *107*(A2), 1029, doi:10.1029/2001JA900104.

Cooling, B. M. A., C. J. Owen, and S. J. Schwartz (2001), Role of the magnetosheath flow in determining the motion of open flux tubes, *J. Geophys. Res.*, *106*, 18,763.

Cowley, S. W. H., J. P. Morelli, and M. Lockwood (1991), Dependence of convective flows and particle precipitation in the high-latitude dayside ionosphere on the X and Y components of the interplanetary magnetic field, *J. Geophys. Res.*, *96*, 5557.

Crooker, N. U., and F. J. Rich (1993), Lobe cell convection as a summer phenomenon, *J. Geophys. Res.*, *98*, 13,403.

Crooker, N. U., J. G. Lyon, and J. A. Fedder (1998), MHD model merging with IMF B_y: Lobe cells, sunward polar cap convection, and overdraped lobes, *J. Geophys. Res.*, *103*, 9143.

Elphinstone, R. D., D. J. Hearn, J. S. Murphree, L. L. Cogger, M. L. Johnson, and H. B. Vo (1993), Some UV dayside auroral morphologies, in *Auroral Plasma Dynamics*, *Geophys. Monogr. Ser.*, vol. 80, edited by R. Lysak, p. 31, AGU, Washington, D. C.

Eriksson, S., J. W. Bonnell, L. G. Blomberg, R. E. Ergun, G. T. Marklund, and C. W. Carlson (2002), Lobe cell convection and field-aligned currents poleward of the Region 1 current system, *J. Geophys. Res.*, *107*(A8), 1185, doi:10.1029/2001JA005041.

Foster, J. C., J.-P. St.-Maurice, and V. J. Abreu (1983), Joule heating at high latitudes, *J. Geophys. Res.*, *88*, 4885.

Frey, H. U., S. B. Mende, C. W. Carlson, J.-C. Gérard, B. Hubert, J. Spann, R. Gladstone, and T. J. Immel (2001), The electron and proton aurora as seen by IMAGE-FUV and FAST, *Geophys. Res. Lett.*, *28*, 1135.

Frey, H. U., S. B. Mende, T. J. Immel, S. A. Fuselier, E. S. Claflin, J.-C. Gérard, and B. Hubert (2002), Proton aurora in the cusp, *J. Geophys. Res.*, *107*(A7), 1091, doi:10.1029/2001JA900161.

Frey, H. U., T. J. Immel, G. Lu, J. Bonnell, S. A. Fuselier, S. B. Mende, B. Hubert, N. Østgaard, and G. Le (2003a), Properties of localized, high latitude, dayside aurora, *J. Geophys. Res.*, *108*(A4), 8008, doi:10.1029/2002JA009332.

Frey, H. U., S. B. Mende, T. J. Immel, J.-C. Gérard, B. Hubert, S. Habraken, J. Spann, G. R. Gladstone, D. V. Bisikalo, and V. I. Shematovich (2003b), Summary of quantitative interpretation of IMAGE far ultraviolet auroral data, *Space Sci. Rev.*, *109*, 255.

Frey, H. U., S. B. Mende, S. A. Fuselier, T. J. Immel, and N. Østgaard (2003c), Proton aurora in the cusp during southward IMF, *J. Geophys. Res.*, *108*(A7), 1277, doi:10.1029/2003JA009861.

Gosling, J. T., M. F. Thomsen, S. J. Bame, R. C. Elphic, and C. T. Russell (1991), Observations of reconnection of interplanetary and lobe magnetic field lines at the high-latitude magnetopause, *J. Geophys. Res.*, *96*, 14,097.

Jacobsen, B., P. E. Sandholt, W. J. Burke, W. F. Denig, and N. C. Maynard (1995), Optical signatures of prenoon auroral precipitation: Sources and responses to solar wind variations, *J. Geophys. Res.*, *100*, 8003.

Jankowska, K., R. D. Elphinstone, J. S. Murphree, L. L. Cogger, and D. Hearn (1990), The configuration of the auroral distribution for interplanetary magnetic field B_z northward: 2. Ionospheric convection consistent with Viking observations, *J. Geophys. Res.*, *95*, 5805.

Korth, H., B. J. Anderson, H. U. Frey, T. J. Immel, and S. B. Mende (2004), Conditions governing localized high-latitude dayside aurora, *Geophys. Res. Lett.*, *31*, L04806, doi:10.1029/2003GL018911.

Kullen, A., M. Brittnacher, J. A. Cumnock, and L. G. Blomberg (2002), Solar wind dependence of the occurrence and motion of polar auroral arcs: A statistical study, *J. Geophys. Res.*, *107*(A11), 1362, doi:10.1029/2002JA009245.

Le, G., G. Lu, R. J. Strangeway, and R. F. Pfaff (2002), Strong interplanetary magnetic field B_y-related plasma convection in the ionosphere and cusp field-aligned currents under northward interplanetary magnetic field conditions, *J. Geophys. Res.*, *107*(A12), doi:10.1029/2001JA007546.

Liou, K., P. T. Newell, C.-I. Meng, T. Sotirelis, M. Brittnacher, and G. Parks (1999), Source region of 1500 MLT auroral bright spots: Simultaneous Polar UV-images and DMSP particle data, *J. Geophys. Res.*, *104*, 24,587.

Luhmann, J. G., R. J. Walker, C. T. Russell, N. U. Crooker, J. R. Spreiter, and S. S. Stahara (1984), Patterns of potential magnetic field merging sites on the dayside magnetopause, *J. Geophys. Res.*, *89*, 1739.

Mende, S. B., et al. (2000), Far ultraviolet imaging from the IMAGE spacecraft, *Space Sci. Rev.*, *91*, 287.

Meng, C.-I. (1981), Polar cap arcs and the plasma sheet, *Geophys. Res. Lett.*, *8*, 273.

Murphree, J. S., and R. D. Elphinstone (1988), Correlative studies using the Viking imagery, *Adv. Space Res.*, *8*(9), 9.

Murphree, J. S., R. D. Elphinstone, D. Hearn, and L. L. Cogger (1990), Large-scale high-latitude dayside auroral emissions, *J. Geophys. Res.*, *95*, 2345.

Newell, P. T., C.-I. Meng, and K. M. Lyons (1996), Suppression of discrete aurorae by sunlight, *Nature*, *381*, 766.

Ohtani, S., R. D. Elphinstone, O. A. Troshichev, M. Yamauchi, L. Blomberg, L. J. Zanetti, and T. A. Potemra (1997), Response of the dayside auroral and electrodynamic processes to variations in the interplanetary magnetic field, *J. Geophys. Res.*, *102*, 22,247.

Papitashvili, V. O., and F. J. Rich (2002), High-latitude ionospheric convection models derived from DMSP ion drift observations and parameterized by the IMF strength and direction, *J. Geophys. Res.*, *107*(A8), 1198, doi:10.1029/2001JA000264.

Papitashvili, V. O., B. A. Belov, D. S. Faermark, Y. I. Feldstein, S. A. Golyshev, and A. E. Levitin (1994), Electric potential patterns in the northern and southern polar regions parameterized by the interplanetary magnetic field, *J. Geophys. Res.*, *99*, 12,251.

Pokhotelov, D., W. Lotko, and A. V. Streltsov (2002), Effects of the seasonal asymmetry in ionospheric Pedersen conductance on the appearance of discrete aurora, *Geophys. Res. Lett.*, *29*(10), 1437, doi:10.1029/2001GL014010.

Sandholt, P. E., C. S. Deehr, A. Egeland, B. Lybekk, R. Viereck, and G. J. Romick (1986), Signatures in the dayside aurora of plasma transfer from the magnetosheath, *J. Geophys. Res.*, *91*, 10,063.

Shue, J.-H., P. T. Newell, K. Liou, and C.-I. Meng (2001), The quantitative relationship between auroral brightness and solar EUV Pedersen conductance, *J. Geophys. Res.*, *106*, 5883.

Siscoe, G. L., and E. Sanchez (1987), An MHD model for the complete open magnetotail boundary, *J. Geophys. Res.*, *92*, 7405.

Siscoe, G. L., G. M. Erickson, B. U. O. Sonnerup, N. C. Maynard, K. D. Siebert, D. R. Weimer, and W. W. White (2001), Global role of $E_{||}$ in magnetopause reconnection: An explicit demonstration, *J. Geophys. Res.*, *106*, 13,015.

Walker, I. K., J. Moen, L. Kersley, and D. A. Lorentzen (1999), On the possible role of cusp/cleft precipitation in the formation of polar-cap patches, *Ann. Geophys.*, *17*, 1298.

Weimer, D. R. (2001), An improved model of ionospheric electric potentials including substorm perturbations and application to the Geospace Environment Modeling November 24, 1996, event, *J. Geophys. Res.*, *106*, 407.

Zhu, L., R. W. Schunk, and J. J. Sojka (1997), Polar cap arcs: A review, *J. Atmos. Solar Terr. Phys.*, *59*, 1087.

H. U. Frey, T. J. Immel, S. B. Mende, and N. Østgaard, Space Sciences Laboratory, University of California, Berkeley, CA 94720-7450, USA. (hfrey@ssl.berkeley.edu)

H. Korth, Applied Physics Laboratory, Johns Hopkins University, Laurel, MD 20723-6099, USA. (haje.korth@jhuapl.edu)